

## The hard X-ray shortages prompted by the clock bursts in GS 1826–238

Long Ji<sup>1</sup>, Shu Zhang<sup>1</sup>, YuPeng Chen<sup>1</sup>, ShuangNan Zhang<sup>1</sup>, Diego F. Torres<sup>2,3</sup>, Peter Kretschmar<sup>4</sup>, Jian Li<sup>1</sup>

### ABSTRACT

We report on a study of GS 1826–238 using all available *RXTE* observations, concentrating on the behavior of the hard X-rays during type-I bursts. We find a hard X-ray shortage at 30–50 keV promoted by the shower of soft X-rays coming from type-I bursts. This shortage happens with a time delay after the peak of the soft flux of  $3.6 \pm 1.2$  seconds. The behavior of hard X-rays during bursts indicates cooling and reheating of the corona, during which a large amount of energy is required. We speculate that this energy originates from the feedback of the type-I bursts to the accretion process, resulting in a rapid temporary increase of the accretion rate.

*Subject headings:* stars: coronae — stars: neutron — X-rays: individual(GS 1826–238) — X-rays: binaries — X-rays: bursts

### 1. Introduction

Low mass X-ray binaries (XRBs) consist of a compact (neutron star or black hole) and a companion star, with the latter transferring mass and forming an accretion disc, a process during which the gravitational potential energy is converted into radiation, see, e.g., Lewin et al. (1993); Strohmayer & Bildsten (2006); Galloway et al. (2008), and references therein. The spectrum is usually modeled having two components: a blackbody plus a power law, in which the former represents the emission of the accretion disc, and the latter is attributed to the contribution of corona or jet (Remillard & McClintock 2006; Markoff et al. 2004). If the hard X-rays are from synchrotron radiation in a jet, one would likely observe too the radio emissions in the lower energy band. However according to radio observations of XRBs, the luminosity of the systems having a neutron star companion is systematically lower than of those having a black hole, by a factor of  $\sim 30$ , and the relation of the radio and X-ray luminosity is different between neutron stars and black holes. Therefore, the hard X-rays in neutron star systems more likely derive from inverse Comptonization processes in a corona (for details, please see Migliari et al. (2010); Migliari & Fender (2006)).

However, although the concept of the corona is widely used in current models, its formation remains less understood. Both, evaporation (Meyer et al. 1994; Esin et al. 1997; Liu et al. 2007; Frank et al. 2002)

---

<sup>1</sup>Laboratory for Particle Astrophysics, Institute of High Energy Physics, Beijing 100049, China

<sup>2</sup>Institució Catalana de Recerca i Estudis Avançats (ICREA), 08010 Barcelona, Spain

<sup>3</sup>Institute of Space Sciences (IEEC-CSIC), Campus UAB, Torre C5, 2a planta, 08193 Barcelona, Spain

<sup>4</sup>European Space Astronomy Centre (ESA/ESAC), Science Operations Department, Villanueva de la Cañada (Madrid), Spain

and magnetic reconnection (Zhang et al. 2000; Mayer & Pringle 2007) models have been proposed. Type-I bursts provide a fresh input of soft-X-ray photons with which the corona electrons could interact, and thus they may become a useful probe. Type-I bursts are thermal nuclear explosions that are triggered by the unstable burning on the surface of the neutron star and characterized by intense emissions released in a short time (generally, several tens of seconds) in the form of a blackbody (Swank et al. 1977). In several other atoll sources, namely IGR J17473-2721, Aql X-1, and 4U 1636-536, a shortage of flux in the hard X-ray band during X-ray bursts has been found (Maccarone et al. 2003; Chen et al. 2013; Ji et al. 2013). GS 1826–238 is an atoll source, exhibiting substantial number of X-ray bursts. It was discovered by the Ginga satellite in 1988 (Makino et al. 1988) and its type-I bursts were first detected by BeppoSAX (Ubertini et al. 1997). The shape and spectrum of bursts in GS 1826-238 change little and the persistent flux is relatively stable (Galloway et al. 2004; Thompson et al. 2005). These properties imply relatively smaller systematic errors when investigating the burst influence when compared with bursts in other sources. In addition, the duration of bursts in GS 1826-238 is much longer than those in other sources, resulting in a more significant shortage in the hard X-rays. Assuming a distance of 6 kpc, this source is always staying in the low hard state with a luminosity of 5% – 9%  $L_{\text{edd}}$ , and a spectrum dominated by a power law (Galloway et al. 2008). What makes this source unique is the remarkable stability of its burst recurrence rate as a function of mass accretion rate over a timescale of many years. GS 1826–238 is also called the ‘clock-burster’ because of this fact (Ubertini et al. 1999). Rossi X-Ray Timing Explorer (*RXTE*) observations revealed that the source flux intensity steadily increased between 1997-2003, during which the burst rate increased. The distance to the source was estimated at 4 – 8 kpc (Barret et al. 1995; in ’t Zand et al. 1999; Kong et al. 2000). Its hard X-ray emissions are usually modeled by a thermal Comptonization with a hot electron cloud ( $T \sim 20$  keV) (Cocchi et al. 2010).

In this paper, we report on a study using all available *RXTE* observations of GS 1826–238, concentrating on the behavior of the hard X-rays during type-I bursts.

## 2. Observations and data analysis

We analyzed the observations of GS 1826–238 carried out by the All Sky Monitor (ASM; Levine et al. 1996) and the Proportional Counter Array (PCA; Jahoda et al. 1996) on board *RXTE*. For the latter, only pointing mode data were used, amounting 912 ks. The PCA was made-up of five identical co-aligned proportional counter units (PCUs) that were sensitive to 2–60 keV photons. We have used all active PCUs during bursts for the following analysis and for each burst we have normalized the lightcurve in unit of counts/s/PCU. We took the Event-mode data when producing the lightcurves, due to its high time resolution. For the persistent flux, the background was created based on the latest bright source models using the program *pcabackest*, which is a standard software in *FTOOLS*. Note that above 30 keV PCA count rates are dominated by the instrument background, which varies substantially during an orbit (Jahoda et al. 1996). But we found that the persistent flux prior to the bursts is consistent with that after bursts, suggesting the background could lead to little influence on the following analysis because of the short duration of bursts. Detector breakdowns were eliminated, and the dead time was corrected according to the data of stan-

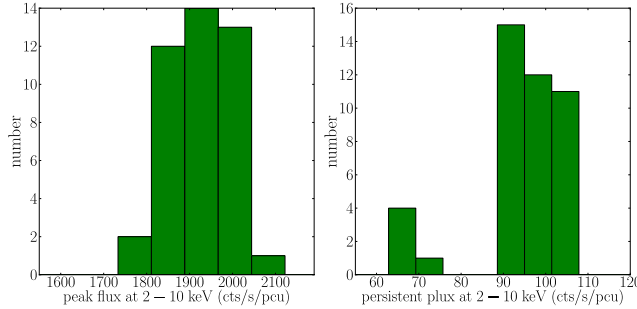


Fig. 1.— The distributions of the persistent and peak fluxes for the type-I bursts

standard 1 mode. The spectrum was fitted by *XSPEC* 12.7.1, fixing the hydrogen column density to  $0.3 \times 10^{22}$  atoms/cm<sup>2</sup> (Thompson et al. 2005).

To distinguish real bursts from fluctuations in the persistent emission, we searched for bursts that presented a peak flux of at least 500 cts/s larger than the persistent flux in the 2–10 keV energy band. As we show in Section 3, the narrow distributions of the persistent and peak fluxes average at  $\sim 94$  cts/s and  $\sim 1917$  cts/s, respectively. Hence, such a selection criterion is reasonable and effective to search for the bursts. We eliminated the bursts for which the observations were incomplete in a time period of 400 seconds around the flux peak (150 seconds before and 250 seconds after). With these cuts, 43 bursts were selected as our sample.

Since the launch of *RXTE* at the end of 1995, GS 1826–238 was observed 160 times in pointing mode. Both PCA and ASM observations showed an increasing luminosity between 1997 and 2003, with the X-ray intensity flattening afterwards.

### 3. Results

We extracted the persistent emission several tens of seconds prior to the bursts, assuming that the accretion rate is unchanged, and fitted the net burst spectrum with the empirical model *wabs* (Morrison & McCammon 1983)  $\times$  *blackbody*. In order to reduce the errors, we defined for each burst its average temperature as the one derived from the data within two seconds around the peak flux. The mean temperature of the 43 bursts is  $2.18 \pm 0.07$  keV. This result is consistent with the works by in ’t Zand et al. (1999); Ubertini et al. (1999); Galloway et al. (2008). After convolving with the response matrix, a spectrum with this temperature would lead to a contribution of at most  $0.24 \pm 0.08$  cts/s in the energy band of 30–50 keV, which is much smaller than the corresponding average of the persistent emission, resulting in  $1.69 \pm 0.02$  cts/s. Therefore, the energy band of 30–50 keV is appropriate for investigating the burst influence upon the hard X-ray emission.

The Event-mode data was used to produce lightcurves with bin size of 1 second. Following *RXTE*’s recommended criterion, the background was estimated by *packbest* using the latest bright source model,

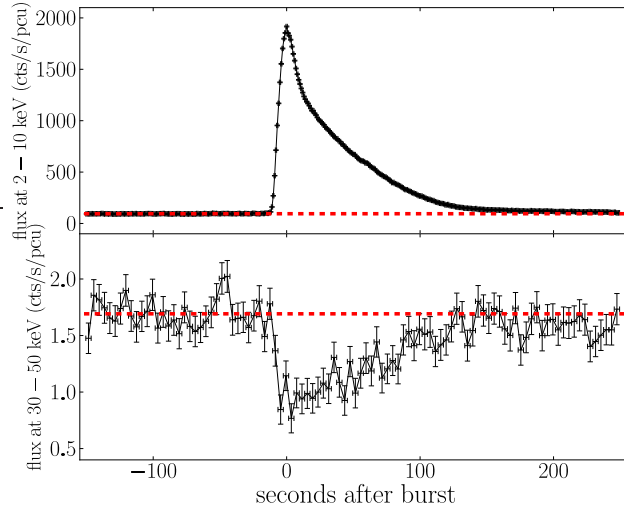


Fig. 2.— The combined lightcurves of all the 43 bursts at energies of 2–10 keV and 30–50 keV.

and subtracted off by the *FTOOLS* command *lcmath*.<sup>1</sup> The properties of these bursts are listed in Table 1, and the distributions of their persistent and peak fluxes are shown in Figure 1. Table 1 shows that throughout the whole *RXTE* era, the bursts were very similar to each other. The persistent flux was estimated as the averaged count rate within the range of 150 to 50 s prior to each burst, and their averages were  $94.79 \pm 0.09$  and  $1.69 \pm 0.02$  cts/s at 2–10 and 30–50 keV, respectively. This result is consistent with the reports of Cocchi et al. (2010) where GS 1826–238 was mostly observed in the hard state with a rather stable spectrum. Hence, we summed up all the bursts in 2–10 keV and 30–50 keV, respectively, in bin sizes of 1s and 4s. In order to do this, we took the peak flux as a time reference for each burst and average the count rate in each bin of the individual lightcurves. The combined lightcurve is shown in Figure 2. There is a significant shortage in the 30–50 keV band along with the burst evolution. If we take the null hypothesis that the hard X-ray shortage derives from statistical fluctuation, a  $\chi^2$  test, assuming the lightcurve can be fitted by a constant line, results in a value of 508.98 under 28 dofs, implying the null hypothesis is unacceptable. The integral flux for the shortage is  $-58.25 \pm 2.76$ , suggesting a significant level of  $\sim 21\sigma$ . This phenomenon is similar to that reported for IGR J17473-2721, 4U 1636-536 and Aql X-1, but at a higher significant level (Chen et al. 2012; Ji et al. 2013; Chen et al. 2013; Maccarone et al. 2003).

Figure 3 shows the burst flux-flux diagram. It is based on the 4 s bin lightcurves. Prior to the bursts, namely when the averaged persistent flux at 2–10 keV is  $94.79 \pm 0.09$  cts/s, the hard X-ray flux in the 30–50 keV band is  $1.69 \pm 0.02$  cts/s. This hard X-ray level is marked with a green line in that figure. When the bursts proceed, there is an anti-correlation between soft and hard X-ray fluxes at least until the soft count rate reaches  $\sim 1000$  cts/s, while the hard X-ray flattens afterwards. These results, however, have to be taken with care due to the large error bars of the hard X-ray flux measurements. To explore the significance of this

---

<sup>1</sup>Note that the background could only be extracted from the data of Standard 2 mode with the bin size of 16 s and employed for Event-mode data. This is a standard procedure, the details are available at <http://heasarc.gsfc.nasa.gov/docs/xte/abc/contents.html>

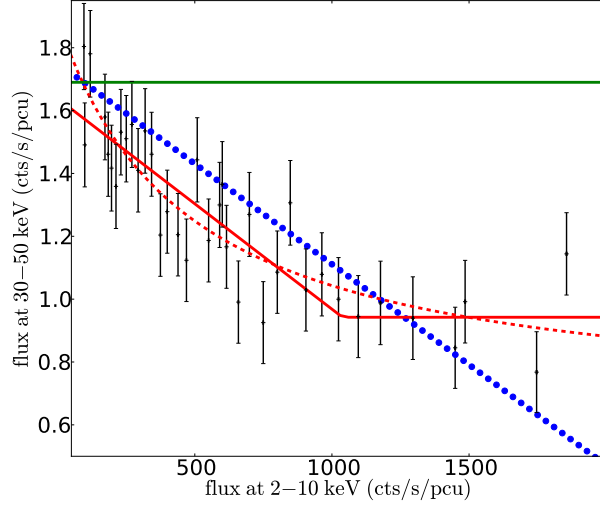


Fig. 3.— Flux-flux diagram corresponding to the energies of 2–10 keV and 30–50 keV. The green horizontal line represents the initial hard X-ray intensity of 1.69 cts/s. The blue point line, the red solid line, and the red dash line show the linear fitting, piecewise fitting, and inverse proportion fitting, respectively.

behavior, we fit the data with a piecewise function ( $ax+b, x < c; ac+b, x > c$ , the solid line in Figure 3) and an inverse proportion function ( $a/(b+x)+c$ , the dash line). For the former, the resulting best fit parameters are  $a = (6.67 \pm 0.66) \times 10^{-4}$ ,  $b = 1.64 \pm 0.04$  and  $c = 1038.47 \pm 424.52$  with a  $\chi^2$  of 32.28 (34 dof); for the latter,  $a = 585.45 \pm 354.54$ ,  $b = 469.27 \pm 275.76$ , and  $c = 0.64 \pm 0.18$ , with a  $\chi^2$  of 29.71 (34 dof). Both of these fits show a significant improvement with respect to a linear fitting (shown in Figure 3).

Because the shape and spectrum of bursts are quite similar and the persistent flux is relatively stable, GS 1826–238 seems so far the best candidate to explore the corona behavior under the influence of the bursts. While bursting, the thermal component of the spectrum should increase, as well as the corresponding normalization of the compton component, because the emitted photons for the former can be regarded as the incident photons of the latter. Meanwhile, the Compton process will take energy away from the corona and lead to a lower coronal temperature. The hard X-ray shortage we observe reveals a mixture of increasing normalization and decreasing temperature. However, limited by the quality of the spectrum, we were unable to estimate both of the variations of the normalization and temperature. Hence, we assumed that the normalization is unchanged while bursting and estimated an upper limit to the corona temperature. In practice, based on the fitting results in Table 3 by Thompson et al. (2005), we estimated the variation of the corona temperature by setting free  $T_e$  (the temperature of the hot electrons in the corona) in *compTT* or  $E_{\text{cut}}$  in *cutoffpl* for which  $E_{\text{cut}} \sim 2 T_e$ . Figure 4 shows the 8-s bin inferred corona temperature as a function of time around the bursts. The different lines in that figure represent different models used (The one is *phabs\*(bbody+cutoffpl+gauss)*, and the other one is *phabs\*(compTT+compTT+gauss)*), the red horizontal line stands for the initial temperature of  $20.79^{+0.72}_{-1.08}$  (Thompson et al. 2005). From Figure 4 we can see that at the peak of the clock bursts the corona may have a temperature  $\sim 10$  keV.

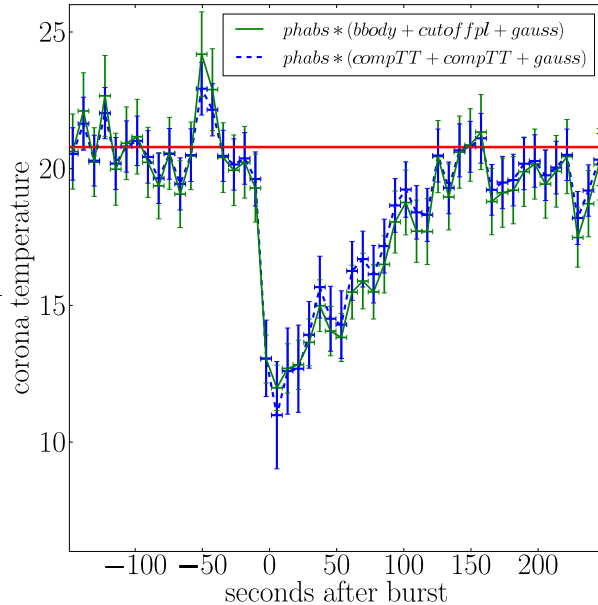


Fig. 4.— The inferred 8-s bin corona temperature versus time around the burst as obtained using different models. The horizontal line represents the initial temperature of 20.79 keV.

To estimate the possible time lag between hard and soft X-rays, we carried out a cross correlation analysis between the lightcurves in two energy bands with 4 s bin size. In practice, to match the peaks more exactly, the data within 20 seconds around bursts (–20s, 20s) are used. The error of the time lag was derived with Monte Carlo via sampling of the lightcurves in these two energy bands, for details see Ji et al. (2013). We obtain a time delay of  $\sim 3.6 \pm 1.2$  s with the cross correlation coefficient  $-0.74 \pm 0.03$ . The value of time delay is consistent in case different bin-size lightcurves are used as well.

## 4. Discussion and summary

We find a hard X-ray shortage in the 30–50 keV band promoted by the shower of soft X-ray photons coming from the type-I bursts in GS 1826–238. This shortage happens with a time delay of  $3.6 \pm 1.2$  seconds after the peak of the soft flux. The latter is somewhat larger and more significant than the shortages found in other sources, for example, IGR J17473-2721, 4U 1636-536, and Aql X-1, where the observed time delays are  $0.7 \pm 0.5$ ,  $2.4 \pm 1.5$  and  $1.8 \pm 1.5$ , respectively.

### 4.1. The feedback of type-I bursts to the accretion process

The cooling and reheating of the corona require an energy budget. We estimate this required energy in terms of inverse Compton scatter:  $E_c = E_{\text{burst}} (e^Y - 1)$ , where  $E_{\text{burst}}$  refers to the nuclear energy

released in a type-I burst, which is  $\sim 5.3 \times 10^{39}$  ergs (Galloway et al. 2004). The dimensionless Y parameter (Rybicki & Lightman 1979) is given by  $\sim \frac{4kT_e}{m_e c^2} \text{Max}(\tau, \tau^2)$ , where  $T_e$  and  $\tau$  are the characteristic temperature and optical depth respectively. By taking  $\frac{3}{2}kT_e$  and  $\tau$  as 10 keV and 1, the resulting  $E_c$  is  $\sim 3 \times 10^{38}$  ergs, i.e, the energy of a mass of  $10^{18}$  g accreting onto the neutron star, assuming characteristic values of 1.4 solar mass and a neutron star radius of 8 km. If throughout the burst, the accretion rate remains unchanged, the energy required for the Compton process can only derive from the gravitational potential energy stored by the mass in the inner accretion disc. Assuming a standard accretion disc with  $\alpha$  parameter  $\sim 0.1$  (Shakura & Sunyaev 1973), the mass in the inner accretion disk of  $\sim 50$  km should be eaten up and a corresponding lower luminosity after bursts is expected to be observed. However, based on our observations, the flux turned out to recover to the pre-burst level along with the evolution of bursts. Therefore, the energy should derive from an increase of accretion rate during bursting, and we estimate the increase is at least 3%  $M_{\text{edd}}$ . This result shows that the feedback of bursts to the accretion process is significant on short timescales of  $\sim 100$  seconds. This result is consistent with the findings of Worpel et al. (2013). Recently, assuming the persistent spectrum remains constant throughout the burst, they proposed a multiplicative factor  $f_a$  to the persistent emissions and took it into spectral fits while bursting. They found that the best-fit value of  $f_a$  was significantly greater than 1, suggesting the persistent flux increases during bursts.

In the accretion process, the accretion rate is limited by the efficiency of angular momentum transfer. The increase of the accretion rate directly points to a requirement of the additional angular momentum transfer. However, Walker & Mészáros (1989) proposed that the Poynting-Robertson drag could be regarded as a large torque on the inner boundary of the accretion disc and cause severe disc depletion: the inner radius of the optically thick disc moved outward. And after the burst peak, radiation-driven angular momentum transfer declines rapidly and the innermost radius of the accretion disc returns to the previous position gradually. Time-dependent numerical simulation has been shown in Figure 3 and 4 of Walker (1992), in which the estimated increase of accretion could be larger than the energy requirement for the recovery of the corona, the remaining energy may contribute to the burst luminosity. In theory, models cannot constrain the regressive distance. In terms of the radial velocity (assuming  $\alpha$  factor  $\sim 0.1$ ) in standard disc (Shakura & Sunyaev 1973) and the characteristic burst duration of 100 seconds for hydrogen ignition and 20 seconds for helium ignition, here we estimated their upper limits as  $\sim 60$  km and  $\sim 10$  km, respectively.

#### 4.2. Detailed formation mechanism of the corona

Based on the observed time lag of seconds between hard and soft X-rays in IGR J17473-2721, Chen et al. (2012) concluded that typical evaporation models would not be favored, because their inferred time delay, according to the viscous timescale (Frank et al. 2002), should be days, which corresponds to complete evaporation of the innermost accretion disc. However, if we consider the influence of the additional angular momentum loss, the estimated time delay should be modified. In classical evaporation models, the coronal evaporation results from the mechanism of "siphon-flow" (for details, see Meyer et al. (1994)). The hot corona above the accretion disc conducts heat downward by electron conduction. Along with the decreasing of the temperature from a high coronal value of  $\sim 10^9$  K (Narayan & Yi 1995) to a low disc level of  $\sim 10^7$

$K$ , heat conduction rate, which is  $\propto T^{2.5}$  (Frank et al. 2002), becomes ineffective. To radiate away the heat, the efficiency of radiation, which depends on the particle number density, should be increasing. As a result, a corona of a given heating rate (or an accretion rate) will "dig" itself into the accretion disc and drain mass from the disc towards the corona. In this process, the key limitation is just the accretion rate, i.e., the rate at which it is able to remove the angular momentum. Therefore, it could be an overestimation to calculate the expected time delay while bursting only as the viscous timescale without considering the angular momentum loss by Poynting-Robertson drag. If to estimate the intrinsic timescale for the "siphon-flow" mechanism the thermal timescale for re-adjustment to thermal equilibrium is used, we obtain  $\sim 0.03$  s under typical parameters of standard disc (Frank et al. 2002). Hence, reasonable enhancements of the evaporation models can not be ruled out as a possible formation mechanism of the corona.

Alternatively, magnetic reconnection models can provide a self-consistent interpretation for the cooling and reheating of the corona. In this scenario, the accretion discs around compact stars are considered in many cases to be threaded by large-scale magnetic field, which may arise from dynamo activities in the disc (Parijev et al. 2007). This large-scale field may form magnetic loops anchored at different radii of the disc and extending the magnetic lines into the corona (Liu et al. 2002). Differential rotation of the disc can open the magnetic loops and magnetic reconnection can heat up the corona (Dyda et al. 2013). Hence, during bursts, while the innermost accretion disc has been depleted (Walker 1992), the magnetic reconnection should stop naturally, to be gradually enhanced again along with the inward movement of the accretion disc.

We acknowledge support from 973 program 2009CB824800 and the Chinese NSFC 11073021, 11133002, 11103020 and XTP project XDA04060604. DFT work is done in the framework of the grants AYA2012-39303 and SGR2009-811, and iLINK2011-0303, and was supported by a Friedrich Wilhelm Bessel Award of the Alexander von Humboldt Foundation. This research has made use of data obtained from the High Energy Astrophysics Science Archive Research Center (HEASARC), provided by NASA Goddard Space Flight Center.

## REFERENCES

- Barret, D., Motch, C., Pietsch, W. 1995, *A&A*, 303, 526B
- Chen, Y. P., Zhang, S., Zhang, S. N., Li, J., Wang, J. M. 2012, *ApJ*, 752, L34
- Chen, Y. P., Zhang, S., Zhang, S. N., et al. 2013, *ApJL*, 777, L9
- Cocchi, M., Farinelli, R., Paizis, A., Titarchuk, L. 2010, *A&A*, 509A, 2C
- Dyda, S., Lovelace, R. V. E., Ustyugova, et al. 2013, *MNRAS*, 432, 127D
- Esin, A. A., McClintock, J. E., Narayan, R. 1997, *ApJ*, 489, 865

- Frank, J., King, A., Raine, J. 2002, *Accretion Power in Astrophysics* (Cambridge: Cambridge Univ. Press)
- Galloway, D. K., Cumming, A., Kuulkers, E., et al. 2004, *ApJ*, 601, 466G
- Galloway, D. K., Munro, M. P., Hartman, J. M., et al. 2008, *ApJS*, 179, 360
- in 't Zand, J. J. M., Heise, J., Kuulkers, E., et al. 1999, *A&A*, 347, 891I
- Jahoda, K., Swank, J. H., Giles, A. B., et al. 1996, *Proc. SPIE.*, 2808, 59J
- Ji L., Zhang, S., Chen, Y. P., et al., 2013, *MNRAS*, 432, 2773
- Kong, A. K. H., Homer, L., Kuulkers, E., Charles, P. A., Smale, A. P. 2000, *MNRAS*, 311, 405K
- Lewin, W. H. G., van Paradijs, J., Taam, R. E. 1993, *Space Sci Rev.*, 62, 223
- Liu, B. F., Mineshige, S., Shibata K. 2002, *ApJ*, 572L, 173L
- Liu, B. F., Taam, R. E., Meyer-Hofmeister, E. 2007, *ApJ*, 671, 695
- Maccarone, T. J., Coppi P. S. 2003, *A&A*, 399, 1151M
- Makino, R., et al. 1988, *IAU Circ.*, 4653, 1
- Markoff, S., Nowak, M. A. 2004, *ApJ*, 609, 972M
- Mayer, M., & Pringle, J. E. 2007, in *AIP Conf. Proc. 924, The Multicolored Landscape of Compact Objects and Their Explosive Origins*, ed. Antonelli L. A. et al. (Melville, NY: AIP), 760
- Meyer, F., Meyer-Hofmeister, E. 1994, *A&A*, 288, 175
- Migliari, S., Fender, R. P. 2006, *MNRAS*, 366, 49M
- Migliari, S., Tomsick, J. A., Miller-Jones, J. C. A., et al. 2010, *ApJ*, 710, 117M
- Morrison, R., McCammon, D. 1983, *ApJ*, 270, 119M
- Narayan, R., Yi, I. 1995, *ApJ*, 452, 710N
- Pariev, V. I., Colgate, S. A., Finn, J. M. 2007, *ApJ*, 658, 129P
- Remillard, R. A., & McClintock, J. E. 2006, *ARA&A*, 44, 49R
- Rybicki, G. B., Lightman, A. 1979, *Radiative Processes in Astrophysics* (Wiley)
- Shakura, N. I., Sunyaev, R. A. 1973, *A&A*, 24, 337S
- Strohmayer, T., & Bildsten, L. 2006, *New views of Thermonuclear Bursts*, ed. Lewin, W. & van der Klis, M. (Cambridge: Cambridge Univ. Press), 113

- Swank, J. H., Becker, R. H., Boldt, E. A., Holt, S. S., Pravdo, S. H., Serlemitsos, P. J. 1977, ApJ, 212L, 73S
- Thompson, T. W. J., Rothschild, R. E., Tomsick, J. A., Marshall, H. L. 2005, ApJ, 634, 1261T
- Ubertini, P., Bazzano, A., Cocchi, M., et al. 1997, IAU Circ., 6111, 1
- Ubertini, P., Bazzano, A., Cocchi, M., et al. 1999 ApJ, 514, L27
- Ubertini, P., Bazzano A., Cocchi, M., et al. 1999, ApL&C, 38, 129U
- Walker, M. A., Mészáros, P. 1989, ApJ, 346, 844W
- Walker, M. A. 1992, ApJ, 385, 642W
- Worpel, H., Galloway, D. K., Price, D. J. 2013, ApJ, 772, 94W
- Zhang, S. N., Cui, W., Chen, W. et al. 2000, Science, 287, 1239

Table 1: The columns denote the observation ID, the time when type-I bursts occurred, peak flux of bursts, soft and hard X-ray persistent flux, and the burst duration.

Observation ID	Modified Julian Day	Peak Flux <sup>a</sup> at 2–10 keV (cts/s/pcu)	Persistent Flux at 2–10 keV (cts/s/pcu)	Persistent Flux at 30–50 keV (cts/s/pcu)	Duration <sup>b</sup> (s)
30054-04-02-01	50971.23	2051.61 ± 20.81	65.87 ± 0.38	1.48 ± 0.12	116
30054-04-02-02	50972.18	2024.11 ± 20.67	66.91 ± 0.39	1.44 ± 0.12	115
30054-04-03-02	50976.42	2026.33 ± 23.14	69.02 ± 0.44	1.49 ± 0.14	116
30060-03-01-01	50988.83	1996.79 ± 22.98	66.12 ± 0.43	1.62 ± 0.14	117
50035-01-01-01	51724.88	1939.21 ± 22.67	89.76 ± 0.50	2.46 ± 0.16	122
50035-01-02-00	51725.71	2022.12 ± 23.06	91.28 ± 0.50	1.58 ± 0.14	123
50035-01-02-00	51725.88	2004.82 ± 23.05	92.43 ± 0.51	2.63 ± 0.16	126
50035-01-02-02	51726.72	1970.52 ± 22.72	92.78 ± 0.50	1.57 ± 0.14	126
50035-01-02-04	51728.77	1976.26 ± 22.78	92.41 ± 0.50	1.53 ± 0.14	125
50035-01-03-00	51811.75	2030.83 ± 26.69	91.32 ± 0.58	1.61 ± 0.16	123
50035-01-03-08	51813.49	1895.19 ± 22.26	90.54 ± 0.50	1.45 ± 0.14	128
50035-01-03-09	51814.01	2018.17 ± 26.79	92.26 ± 0.59	1.30 ± 0.17	130
50035-01-03-10	51814.35	2039.81 ± 32.70	95.46 ± 0.73	1.51 ± 0.21	127
70044-01-01-00	52484.57	1998.33 ± 26.39	104.70 ± 0.61	1.77 ± 0.16	123
70044-01-01-02	52485.01	1961.22 ± 26.21	106.85 ± 0.62	1.84 ± 0.16	136
80048-01-01-00	52736.53	1890.84 ± 25.75	96.70 ± 0.60	1.36 ± 0.17	123
80048-01-01-04	52738.48	1904.97 ± 25.87	94.46 ± 0.59	0.98 ± 0.16	124
80048-01-01-07	52738.61	1779.96 ± 21.66	92.98 ± 0.51	1.27 ± 0.14	133
80048-01-01-07	52738.75	1879.88 ± 22.19	94.69 ± 0.51	1.22 ± 0.13	126
80049-01-01-00	52820.56	1850.85 ± 22.08	96.37 ± 0.51	1.91 ± 0.14	135
80049-01-03-02	52834.39	1915.61 ± 26.08	99.22 ± 0.61	1.51 ± 0.17	133
80049-01-03-03	52835.31	1947.30 ± 22.65	98.37 ± 0.52	1.51 ± 0.14	129
80049-01-02-00	52944.40	1949.54 ± 26.06	93.18 ± 0.58	1.44 ± 0.16	127
70044-01-02-00	53205.20	1879.31 ± 25.77	103.15 ± 0.62	1.46 ± 0.17	131
70044-01-02-01	53206.06	1913.51 ± 25.84	101.22 ± 0.60	1.79 ± 0.16	128
90043-01-01-02	53206.64	2039.15 ± 26.69	99.44 ± 0.60	1.38 ± 0.16	124
90043-01-01-01	53207.22	1913.53 ± 25.88	103.23 ± 0.61	1.75 ± 0.16	135
92703-01-04-02	53951.25	1864.40 ± 44.27	100.58 ± 1.04	2.93 ± 0.29	135
92031-01-02-00	53959.44	1472.39 ± 27.81	75.66 ± 0.64	1.43 ± 0.19	130
90043-01-02-01	53962.58	1833.93 ± 25.33	104.10 ± 0.61	1.89 ± 0.17	134
90043-01-02-01	53962.72	1872.21 ± 25.59	102.83 ± 0.61	1.98 ± 0.16	130
90043-01-02-001	53963.28	1922.97 ± 44.86	96.81 ± 1.02	2.28 ± 0.28	128
90043-01-02-001	53963.42	1746.59 ± 30.24	98.29 ± 0.73	1.87 ± 0.20	132
90043-01-02-00	53963.56	1848.28 ± 44.01	98.99 ± 1.03	1.23 ± 0.28	128
90043-01-03-000	53965.93	1946.33 ± 26.08	104.11 ± 0.61	1.58 ± 0.16	130
70044-01-04-00	53966.37	1848.82 ± 25.39	102.15 ± 0.61	2.00 ± 0.16	138
90043-01-03-01	53966.51	1815.25 ± 30.89	93.73 ± 0.71	1.99 ± 0.21	129
90043-01-03-01	53966.66	1912.50 ± 44.77	97.85 ± 1.02	1.55 ± 0.28	129
91017-01-01-05	54167.58	1846.81 ± 31.19	94.73 ± 0.71	1.78 ± 0.19	125
91017-01-02-03	54168.32	1879.08 ± 31.47	94.75 ± 0.71	1.67 ± 0.19	134
91017-01-02-11	54168.46	1927.11 ± 31.75	104.66 ± 0.75	1.64 ± 0.19	134
91017-01-02-01	54169.05	1824.74 ± 25.23	102.31 ± 0.61	1.88 ± 0.17	135
91017-01-02-09	54169.34	2032.24 ± 32.70	105.68 ± 0.76	1.50 ± 0.20	129

<sup>a</sup>The peak flux is calculated without subtracting persistent flux.

<sup>b</sup>We define the duration of bursts as the time when the flux is larger than 10 % peak flux.